Journal of Korean Society of
Coastal and Ocean Engineers
Vol. 9, No. 4, pp. 194~200, December 1997

Numerical Computation of Unsteady Flow in a Cavity Induced by an Oscillatory External Flow
외부유동에 의한 캐버티 내의 비정상 유동에 대한 수치계산

Yong-Kweon Suh*, Yoon-Hwan Choi*, Jun-Gwan Park* and Jong-Choon Moon**
서용권* · 최윤환* · 박준관* · 문종춘**

Abstract □ A two-dimensional shallow-water flow around a cavity driven by a sinusoidally oscillating external flow was studied numerically. A container model of "T" shape was constructed in the numerical computation for comparison with the experimental observation. The numerical computation shows that the aspect ratio of the cavity is not much affecting the overall flow pattern, and for the aspect ratio 2, the deep region of the cavity has a stagnant flow motion. At larger Reynolds number, the flow field is characterized by many small vortices which are not present in the flow visualization. The flow pattern in the external region is in good agreement with the experimentally recorded particle trajectories. It turns out that two large coherent vortices situated in the exterior region of the cavity are responsible for clockwise and counterclockwise drift motions, in large scale, of particles.

Keywords : cavity, numerical computation, vortex, Ekman pumping effect, Reynolds number

要　旨 : 주기적으로 요동하는 외부유동에 의해 생성되는 캐버티 주위의 2차원 천수유동을 수치적으로 연구하였다. 실험결과와 비교하기 위해 T형의 용기모델을 수치적으로 계산하여 만들었다. 수치계산에서는 캐버티의 종횡비가 전체적인 유동패턴에 크게 영향을 끼치지 않고 종횡비 2에서는 캐버티의 깊은 부분에 정체된 유동형태가 생성되는 것을 제시한다. 높은 레이놀즈 수에서 유동을 가시화 시켰을 때 나타나지 않았던 많은 와류들이 유동장을 특성화 시키고 있다. 외부지역에서의 물질전달은 실험에서 나타난 입자궤적과 잘 일치한다. 캐버티의 외부지역에 위치한 두 쌍의 와류가 규모가 큰 시계방향과 반시계방향의 순환유동을 발생시키는 원인이 되는 것이 증명된 셈이다.

핵심용어 : 함몰부, 수치계산, 와도, 에크만 분출효과, 레이놀즈수

1. INTRODUCTION

In this study, we numerically analyzed two-dimensional flow patterns in a rectangular cavity subject to an external forcing. Fig. 1 shows the geometry of the model basin. In this figure, region ① corresponds to the cavity and region ② is referred to as 'external'. The whole flow field is subject to a sinusoidal forcing to the x^* direction. This model is thought to similitude a bay with an external tide of standing-wave type. The Suh *et al.* (1996) has performed experimental visualization for this model. Except for this, no other informations are available at this time concerning the present flow model. However, some literatures have been recorded for the case when the external flow is replaced by a sinusoidally moving lid (Soh and Goodrich, 1988; Iwatsu *et al.*, 1993; Hyun, 1994). On the other hand, Suh (1996) has shown that flow

*동아대학교 기계공학과 (Department of Mechanical Engineering, Dong-A University, 840 Hadan-dong, Saha-gu, Pusan 604-714, Korea)
**경동전문대학 건축설비과 (Department of Building Equipment Engineering, Kyung-Dong Junior College, 224-1 Buho, Hayang, Kyongsan, 712-900, Korea)

patterns can be asymmetric at Reynolds numbers higher than those the previous studies. There are two objectives in this research; one is to clarify the flow pattern, with variation of external force parameter, and the other is to understand the mass transport pattern in the actual basin affected by a tidal current of standing-wave type.

2. FORMULATION AND NUMERICAL METHODS

Using a shallow-water approximation we obtain the governing equations for two-dimensional incompressible viscous flow as follows:

$$\frac{\partial u^*}{\partial x^*}+\frac{\partial v^*}{\partial y^*}=-\bar{w}^* \tag{1}$$

$$\frac{\partial u^*}{\partial t^*}+u^*\frac{\partial u^*}{\partial x^*}+v^*\frac{\partial u^*}{\partial y^*}=-g\frac{\partial \eta^*}{\partial x^*}+\nu\,\Delta^{*2}u^*+g\,\nabla\theta\cos\omega t^* \tag{2}$$

$$\frac{\partial v^*}{\partial t^*}+u^*\frac{\partial v^*}{\partial x^*}+v^*\frac{\partial v^*}{\partial y^*}=-g\frac{\partial \eta^*}{\partial x^*}+\nu\,\nabla^{*2}v^* \tag{3}$$

$$\frac{\partial \eta^*}{\partial t^*}+\frac{\partial (u^*\,\eta^*)}{\partial x^*}+\frac{\partial (v^*\,\eta^*)}{\partial y^*}=\bar{w}_0^* \tag{4}$$

$$\nabla^{*2}=\frac{\partial^2}{\partial x^{*2}}+\frac{\partial^2}{\partial y^{*2}} \tag{5}$$

where u^*, v^* are the velocity of the x, y-direction, η^* is the liquid height. For numerical computation, we have to nondimensionalization of the governing equations. Nondimensional equation of the paramenters are as follows:

$$(x^*, y^*)=l\,(x, y),\ z^*=hz \tag{6a}$$

$$t^*=\frac{1}{\omega}t \tag{6b}$$

$$(u^*, v^*)=V_g\,(u, v),\ \bar{w}_0^*=\varepsilon V_g\,\bar{w}_0 \tag{6c}$$

$$\eta^*=h\,(1+\eta) \tag{6d}$$

Using a nondimensional equation we obtain the dimensionless governing equations for two-dimensional incompressible viscous flow as follows:

$$\frac{\partial u}{\partial t}+b\left(u\frac{\partial u}{\partial x}+v\frac{\partial u}{\partial y}\right)=-c\frac{\partial \eta}{\partial x}+\frac{1}{\mathrm{Re}}\nabla^2u+d\cos t \tag{7}$$

$$\frac{\partial v}{\partial t}+b\left(u\frac{\partial v}{\partial x}+v\frac{\partial v}{\partial y}\right)=-c\frac{\partial \eta}{\partial y}+\frac{1}{\mathrm{Re}}\nabla^2v \tag{8}$$

$$\frac{\partial \eta}{\partial t}+b\left[\frac{\partial u(1+\eta)}{\partial x}+\frac{\partial v(1+\eta)}{\partial y}\right]=0 \tag{9}$$

where η is the dimensionless liquid height and all the other variables follow the usual convention. The external force dcost present in the right-hand side of (1) drives the flow field and the bottom friction was ignored.

Dimensionless parameters are

$$b=\frac{V_g}{\omega l}=\frac{V_gT^*}{2\pi l} \tag{10a}$$

$$c=\frac{ghT^*}{2\pi V_g l} \tag{10b}$$

$$d=\left(\frac{l}{c^*}\cdot\frac{\Delta h}{h}\right)c \tag{10c}$$

$$\mathrm{Re}=\frac{2\pi l^2}{\nu T^*} \tag{10d}$$

where V_g is a reference velocity (to be defined below), ν is kinematic viscousity, T^* is period, h is the average of liquid height, l is width of the cavity (Fig. 1), ω is angular velocity, g is the acceleration of gravity, and c^* is half of the basin length in region ② (Fig. 1). Assuming a very slow driving force, Δh corresponds to the amplitude of the liquid free surface at both ends of the external basin (Fig. 1). Velocities are nondimensionalized by V_g, which is the maximum velocity for the case of quasi-steady state without the cavity, i. e. $V_g=\pi c^*\Delta h/(T^*h)$. The horizontal coordinates are made dimensionless by the length l, and the vertical coordinate by the depth h. Time is scaled by $1/\omega$, pressure by ρgh, and liquid height funtion (corresponding to η) by h. The dimensionless period then becomes $T=2\pi$. In this study, we fixed all the geometric parameters except for a; we considered two cases, a=1 and a=2. The other parameter changed is Re; two cases studied are Re=8000 and 14000. We also fixed the parameters b, c, and d as b=0.125, c=99, and d=4, respectively; these are calculated from the set, T^*= 5 sec, h=2 cm, l=10 cm, c^*=25 cm, Δh=0.2 cm, and

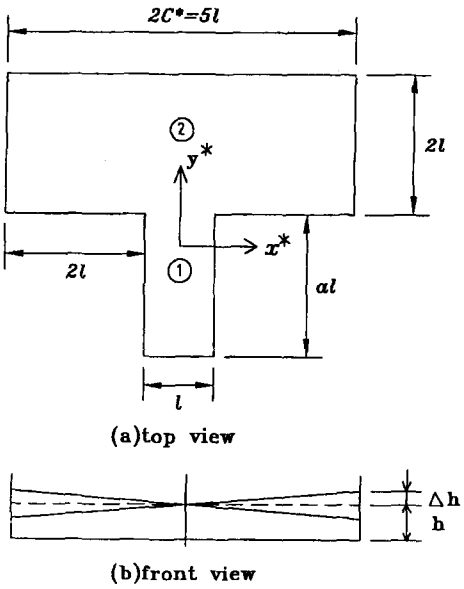

Fig. 1. Geometry of the model basin and the variation of the water level.

thus V_g=1.75 cm/sec.

Boundary conditions are as follows:

$$u = v = 0 \text{ at all side walls} \tag{11}$$

Initial conditions are

$$u = v = 0,\ \eta = \frac{d}{c}x \tag{12}$$

In this study, solution algorithm is based on the fourth order Runge-Kutta method. All the spatial derivatives are discretized by employing the central difference formula. A variable staggered grid system is used. Details of the numerical scheme has been presented elsewhere (Suh and Moon, 1993; Moon, 1993).

3. RESULTS AND DISCUSSIONS

Shown in Fig. 2 is the numerical results of stream and vorticity patterns for a=1 and Re=8000. In this paper, the stream plots mean particle trajectories with frozen velocities at an instant. We see that for one complete cycle, two vortices are present in the cavity; the clockwise (bright one; -sign) in the right-hand side and the counterclockwise (dark one; +sign) in the left-hand side. We also note two larger but weaker vortices in the external region. Since usally the external flow is

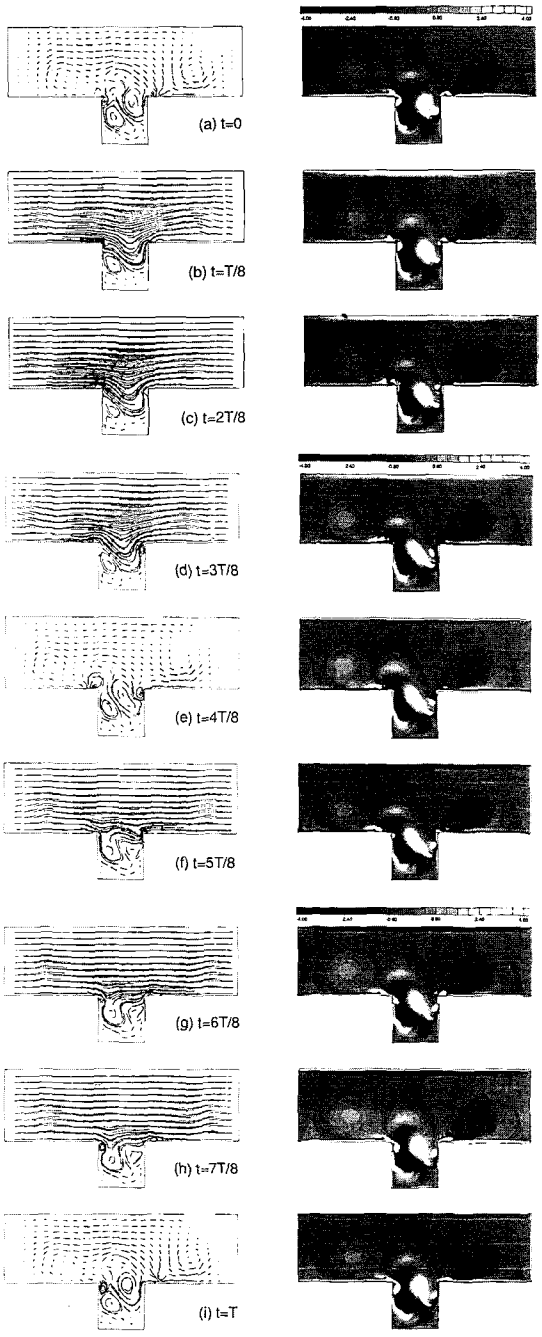

Fig. 2. Stream (left column) and varticity (right column) plots for a=1 and Re=8000. There are numerical results for one period after 30 periods. Each trajectory in the stream plots corresponds to particle trajectory for unit nondimensional time step. Vorticity larger than 4 and smaller than -4 is colored as white and black, respectively.

strong, these latter vortices are not easily identified by the stream plots except at t=0 or $T/2$, when the external current is almost zero. During the first half period, the external current is directed to the left-hand side. Two new vortices with - sign are generated during this period (seen at t=2T/8); one is from the left-hand side's edge and the other from the right-hand side's edge. The former is shed after t=4T/8 and merged with the inner - vortex, and the latter is merged with the outer - vortex. Similarly two + vortices generated from the edges are merged with the two + vortices present in the inner and outer regions. This merging mechanism acounts for the coherent structure of those four large vortices.

Fig. 3 is a sketch explaining the process of vortex generation and its subsequent merging. Shown in Fig. 4 is for the same *Re* as Fig. 2 but at larger a (=2). The whole pattern is similar to Fig. 2. In particular, we see that the deeper half region of ① has almost stagnant flows.

At *Re*=14000 and a=2 (Fig. 5), the flow becomes far more complex. This complexity of course stems from higher *Re*. We shall see that although this is in the same Reynolds number as the experiment, the flow pattern is in worse agreement with the experiment than that of Fig. 2.

The experimental result of flow visualization obtained by Suh *et al.*, 1996, is shown in Fig. 6 for T^*=4.5 sec. The horizontal body force is built by tilting the basin sinusoidally. At this setup, b=0.29, c=51.7, d=2.46, *Re*=13963. Comparing Fig. 6 and either Fig. 4 or Fig. 5, however, we see that Fig. 4 is in better agreement with Fig. 6 although the parametric setup of Fig. 5

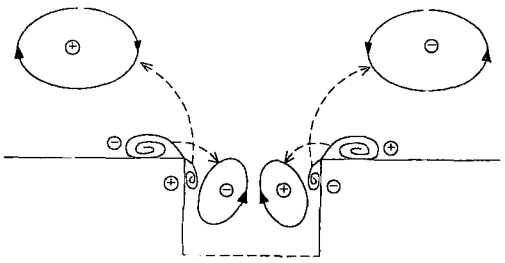

Fig. 3. Sketch for generation (shown as spiral curve) of votices and their subsequent drift motion (shown as dashed line) around the edges of the cavity.

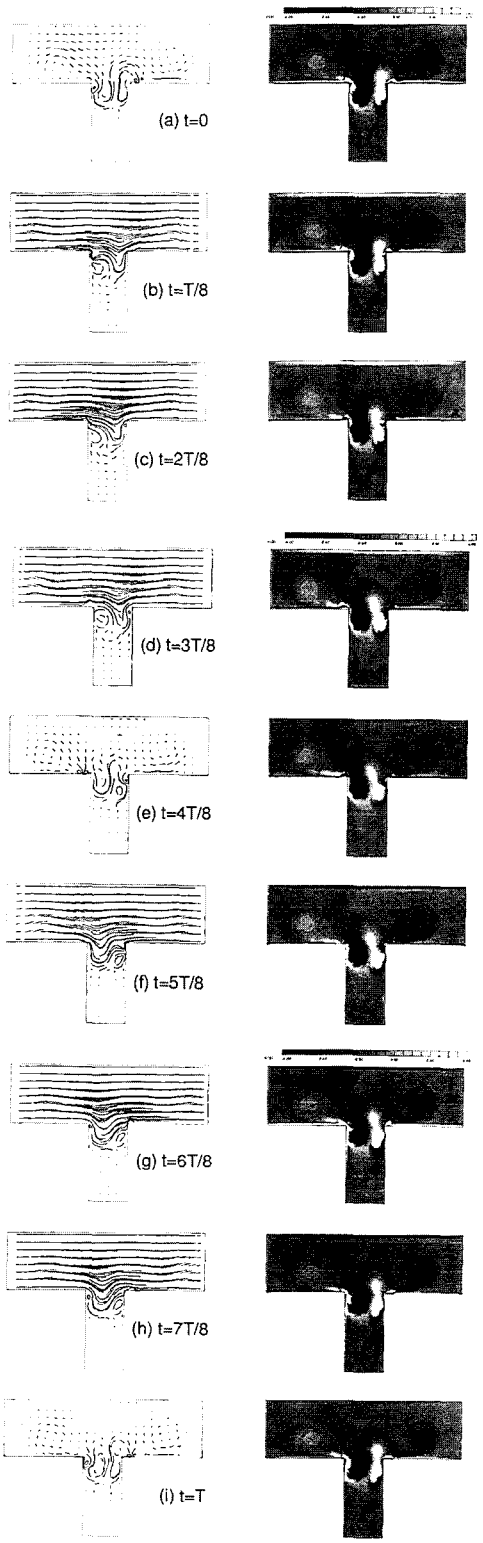

Fig. 4. Same as Fig. 2 except for a=2.

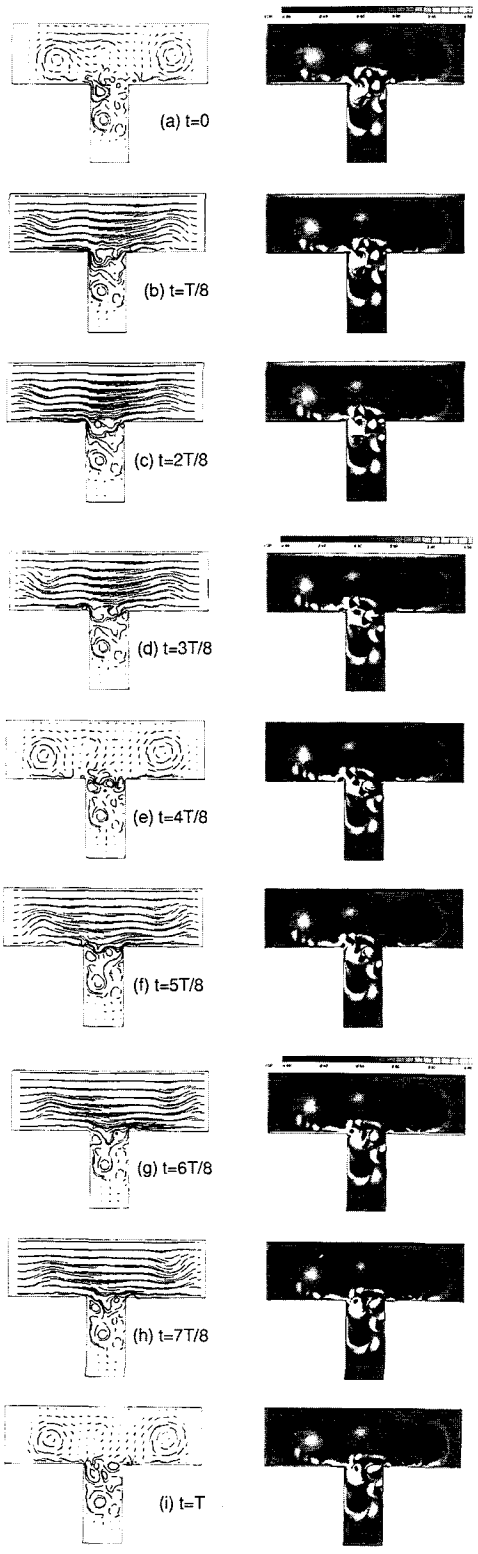

Fig. 5. Same as Fig. 2 except for Re=14000.

is closer to Fig. 6 than Fig. 4. This implies that many small vortices predicted in the numerical computation must be dissipated through the action of bottom frictions or due to the Ekman pumping effect. Further studies are in progress to develop a suitable model to take this effect into acount. We further note that two large vortices present in the cavity predicted by the numerical computation (Fig. 4) are not believed to exist in Fig. 6. Since these vortices do not reside in the experiment, the vortices generated from the edges are resultantly bigger in size than those predicted by the numerical computation. This means that these two vortices are also to be dissipated through the bottom friction effect.

The flow pattern in the external region is, however, in good agreement between the numerical prediction (Fig. 7) and the experimental measurement (Fig. 8). Plotted in Fig. 7 are the vector plots of the velocity field averaged over the last 10 periods among the initial 30 periods of computation. We note that the right-hand side of the external region is, in all cases, characterized by a counterclockwise drift motion, whereas the left-hand side by a clockwise motion. The experimental result for particle trajectories, shown in Fig. 7, also shows clockwise motion in the left-hand side of the outer region. Although not shown in this figure, the right-hand side region is observed to be dominated by a counterclockwise motion as predicted by the numerical computation. We can see that the fundamental cause for the twin circulatory drift motion in the external region is the two coherent vortices residing in each side.

Detecting such coherent vortices from the visualized pattern (i.e. Fig. 6) is not easy since such coherent motion is weaker than the uni-directional external current.

In the actual basin, it is not evident if such large coherent vortices may exist in the exterior region, because absence of the outer three walls will not in general block the region; in fact, one may suspect that without those walls such voticies can not be coherently formed. It is desired to investigate flow patterns for larger external region with a bottom-friction model.

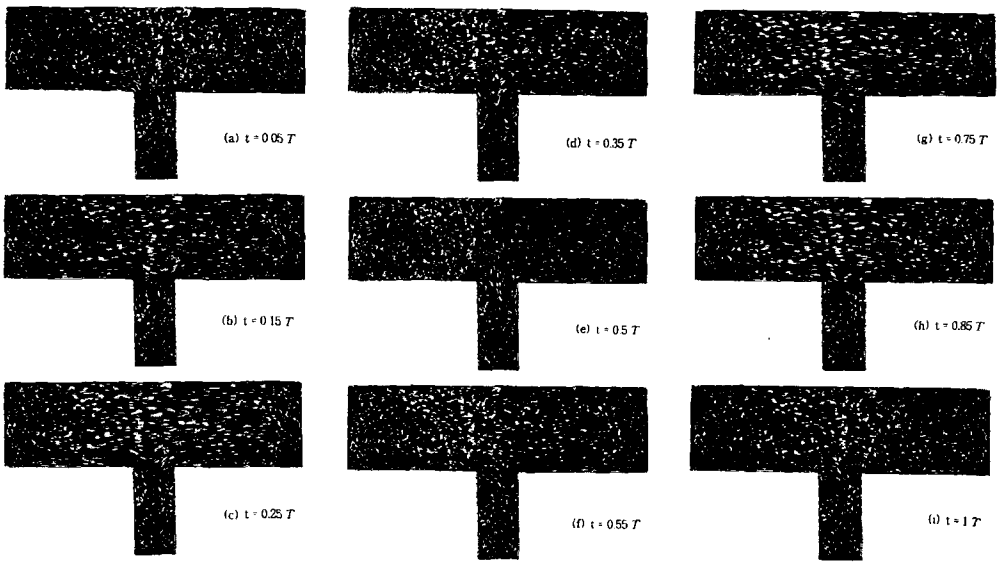

Fig. 6. Surface flow visualization.

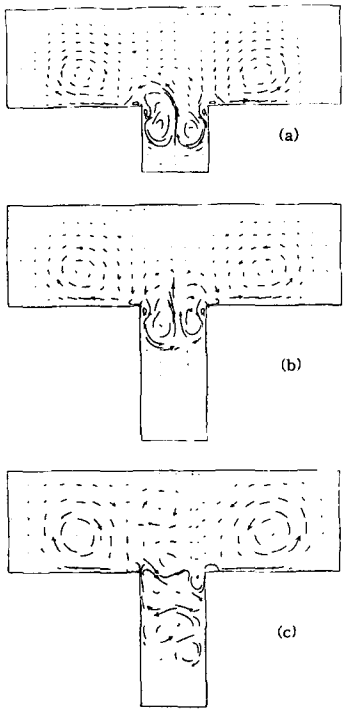

Fig. 7. Stream traces for the velocity field averaged for the last 10 period among the initial 30 periods of computation in the parameter set given in Fig. 3, 4, amd 5; (a) a=1, Re=8000; (b) a=2, Re=8000; (c) a=2, Re=14000.

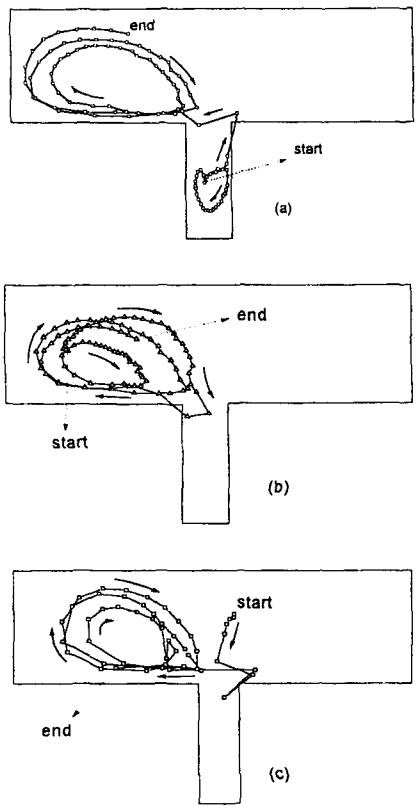

Fig. 8. Trajectory of a particle marked at t=0, T, $2T$, ···, $100T$ for T=4.5 sec.

4. CONCLUSIONS

Numerical computation for the two-dimensional shallow-water flow around a cavity excited by a sinusoidally moving external flow was performed for a model.

We can summarize important findings for this flow model as follows.

(1) The vortices generated from the two edges at the open side of the cavity move to the external as well as the internal region of the cavity and merge with large coherent vortices. These periodically generated vortices move to the other sides, that is, those generated toward inside drift to the external region and those generated toward outside move to the cavity region.

(2) As Reynolds number is increased, many small vortices are present in the flow field making the structure very complicated. These small vortices are not, however, observed in the experimental visualization, and futher studies are necessary to consider bottom friction effects.

(3) The material transport in the external region turns out to be largely affected by the coherent vortices, and the pattern is in good agreement with the experimental investigation.

ACKNOWLEDGEMENT

This study has been supported by Korea Ministry of Education through Mechanical Engineering Research Fund (ME95-B-03).

REFERENCES

Hyun, J.M., 1994. Unsteady buoyant convection in an enclosure, *Advances in Heat Transfer*, **24**, pp. 277-320.

Iwatsu, R., Hyun, J.M. and Kuwahara, K., 1992. Numerical simulation of flows driven by a torsionally oscillating lid in a square cavity, *Trans. ASME J. Fluids Engnrg.*, **114**, pp. 143-151.

Iwatsu, R., Hyun, J.M. and Kuwahara, K., 1993. Numerical simulation of three-dimensional flows in a cubic cavity with an oscillating lid, *Trans. ASME J. Fluids Engnrg.*, **115**, pp. 680-686.

Moon, J.C., 1993. Fluid flow and stirring by vortex shedding in a rectangular tank, *Ph.D. Thesis*, Dong-A University, Pusan, Korea.

Soh, W.H. and Goodrich, J.W., 1988. Unsteady solution of incompressible Navier-Stokes equations, *J. Comput. Phys.*, **79**, pp. 113-134.

Suh, Y.K., 1997. Comparison of multi-stage explicit methods for numerical computation of the unsteady Navier-Stokes equations, *J. Korean Soc. of Mechanical Engineers*, **21**(2), pp. 202-212 (in Korean).

Suh, Y.K. and Moon, J.C., 1993. The flow characteristics in a shallow rectangular tank by vortex shedding, *J. Korean Soc. of Mechanical Engineers*, **17**(8), pp. 2122-2130 (in Korean).

Suh, Y.K., Park, J.K. and Moon, J.C., 1996. Unsteady flow in a cavity induced by an oscillatory external flow, *J. Ocean Engnrg. Tech.*, **10**(3), pp. 105-116 (in Korean).